

Spin echoes in the ground and an optically excited state of $^{167}\text{Er}^{3+}:\text{Y}_2\text{SiO}_5$ at near-zero magnetic fields using Raman heterodyne spectroscopy

Jelena V. Rakonjac,¹ Yu-Hui Chen,¹ Sebastian P. Horvath,^{1,2} and Jevon J. Longdell¹

¹*The Dodd-Walls Centre for Photonic and Quantum Technologies, Department of Physics, University of Otago, 730 Cumberland Street, Dunedin, New Zealand.*

²*Department of Physics, Lund University, P.O. Box 118, SE-22100 Lund, Sweden.*

(Dated: December 14, 2024)

Erbium-167-doped yttrium orthosilicate is an ideal candidate for a microwave-addressed quantum memory due to its telecom wavelength optical transition and hyperfine structure with and without an applied magnetic field. However, to date there has been little investigation in coherence times for transitions around zero magnetic field, or for hyperfine structure other than from the ground state. Through the use of Raman heterodyne spectroscopy, we have identified transitions at zero magnetic field with a small dependence on field that are suitable for detecting spin echoes for both the ground and excited state. We measured coherence times of transitions at 879.4 MHz and 896.7 MHz as 370 μs and 1.4 ms respectively at 3.2 K. This is a 100-fold increase in coherence time compared to previous measurements at the same dopant concentration and 200 times greater than the even isotopes of erbium-doped yttrium orthosilicate previously used to demonstrate a microwave memory.

Rare-earth ion doped crystals are attractive candidates for making quantum memories in addition to other quantum information applications due to their long coherence times for both optical [1] and spin [2] transitions. Transitions with zero first-order Zeeman shift (ZEFOZ) [3] have been shown to give very long coherence times, such as 6 hours for the nuclear spins of europium-151-doped yttrium orthosilicate (Y_2SiO_5) [2].

Long spin coherence times are favorable for applications like quantum memories, but other aspects of the system must be considered for practical implementations. Ideally, the rare-earth ion should possess an optical transition in the telecommunications band. Erbium ions (Er^{3+}) have a unique optical transition at 1.5 μm , allowing the direct use of existing telecommunications infrastructure. In particular, erbium-doped yttrium orthosilicate ($\text{Er}^{3+}:\text{Y}_2\text{SiO}_5$) is of interest as the yttrium ions are the only species in the host material, Y_2SiO_5 , that possess a magnetic moment (aside from uncommon isotopes of silicon and oxygen) [4]. This reduces dephasing of the doped ions due to the host lattice.

However, Er^{3+} is a Kramers' ion - it has an unpaired electron. As a result, the magnetic moment of erbium is larger than that of non-Kramers' ions like europium, inhibiting its coherence time. This can be counteracted by applying a large external magnetic field, as demonstrated by Rančić *et al.* [5], where a 7 T field and cooling to a temperature of 1.4 K was used to freeze out the electron spin and obtain a coherence time of 1.3 s in the hyperfine levels of the isotope erbium-167 doped in yttrium orthosilicate ($^{167}\text{Er}^{3+}:\text{Y}_2\text{SiO}_5$). It can also be counteracted by lowering the temperature, as was demonstrated in $^{166}\text{Er}:\text{LiYF}_4$ [6].

Instead of applying a large magnetic field, we wish to maximize the coherence time of $^{167}\text{Er}^{3+}:\text{Y}_2\text{SiO}_5$ with zero external magnetic field. This would allow compatibility with superconducting qubits, and other supercon-

ducting resonant systems [7]. Erbium-167 has a nuclear spin of 7/2 and an effective electron spin of 1/2, resulting in 16 hyperfine levels in the lowest doublet of the $^4I_{15/2}$ ground state. The measurements made at high fields in Ref. [5] utilized transitions between two states with good quantum numbers of nuclear spin. Unlike at high fields, at low fields the electron and nuclear spin states are mixed. Therefore low-field transitions can occur between different electron spin states and thus have much stronger transition strengths than nuclear spin states and are more suitable for microwave-addressed quantum memories.

Electron paramagnetic resonance (EPR) techniques have been used to measure the coherences times of 4.4 μs and 5.6 μs with a field of 246 mT at 1 K and 30 mK [8] respectively and coherent Raman beat measurements identified a sublevel coherence with a coherence time of at least 50 μs [9] at zero magnetic field.

The coherence time of $^{167}\text{Er}^{3+}:\text{Y}_2\text{SiO}_5$ can be extended by using ZEFOZ points, which exist from zero field to high field. In order to determine the location of ZEFOZ points, an accurate model of the energy levels in the form of a spin Hamiltonian is required. Unfortunately standard continuous wave EPR signals that have been used to characterize the spin Hamiltonian to date [10, 11] disappear at ZEFOZ transitions, inhibiting the modelling of these transitions.

Instead, Raman heterodyne spectroscopy [12, 13] can be used to characterize the hyperfine structure as it is capable of measuring ZEFOZ transitions from anti-crossings that would otherwise not be detected [11] and it works even at zero field unlike conventional EPR. It has been used to characterize many non-Kramers' systems [14–18], and can be used to measure spin echoes [12, 13]. We have previously shown that Raman heterodyne can also be used on Kramers' ions [19].

In this Letter we perform Raman heterodyne spectroscopy on $^{167}\text{Er}^{3+}:\text{Y}_2\text{SiO}_5$ at low fields and demon-

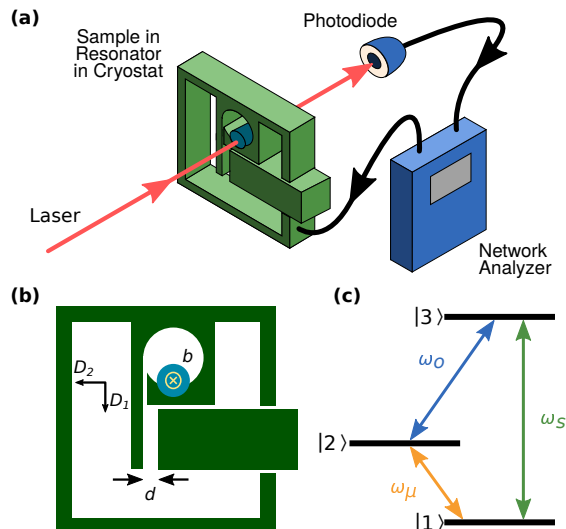


FIG. 1. (a) Experimental setup for continuous wave Raman heterodyne measurements; (b) simplified cross-section of the loop-gap resonator used in the experiments; (c) energy level diagram for Raman heterodyne measurements. A hyperfine transition in the ground or excited state is driven at the frequency ω_μ , with the laser at a frequency of ω_o driving the transition between the ground and excited state and generating an optical field at the sum of the two frequencies, ω_s , as well as the difference between them.

strate the utility of Raman heterodyne for detecting spin echoes from both the electronic ground and $^4I_{13/2}$ excited state. We measure hyperfine structure from both the ground and excited states, which is useful for modifying or determining spin Hamiltonian parameters for both states, particularly the seldom studied excited state.

For our experiments, we use a cylindrical $^{167}\text{Er}^{3+}:\text{Y}_2\text{SiO}_5$ sample (Scientific Materials Inc.), which has a length of 12.0 mm and a diameter of 4.95 mm. 50 parts per million of the Y^{3+} ions are substituted with $^{167}\text{Er}^{3+}$ ions, which can be found in either of two crystallographic sites. Each of the two sites occurs in two different orientations related by the crystal's C_2 (or b) axis and our setup only detects transitions from what is referred to as site 1 [20]. As is convention for this material we use the coordinate system defined by the principle axes of polarization, D_1 , D_2 , and b [21].

The sample is placed inside a tunable microwave resonator [Fig. 1 (b)] made from aluminum, which is based on a single-loop, single-gap design [22]. The resonant frequency can be changed by adjusting the position of a plunger to vary the size of the gap d , similarly to Ref. [23]. The resonant frequency of this particular cavity can be tuned in a range of about 700 MHz to 1200 MHz.

Inside the resonator, the sample is oriented as shown in Fig. 1 (b). A small misalignment of the D_1 and D_2 axes from the horizontal and vertical axes of resonator is to be expected, but this has not been measured. At resonance, the radio frequency (RF) magnetic field oscillates along

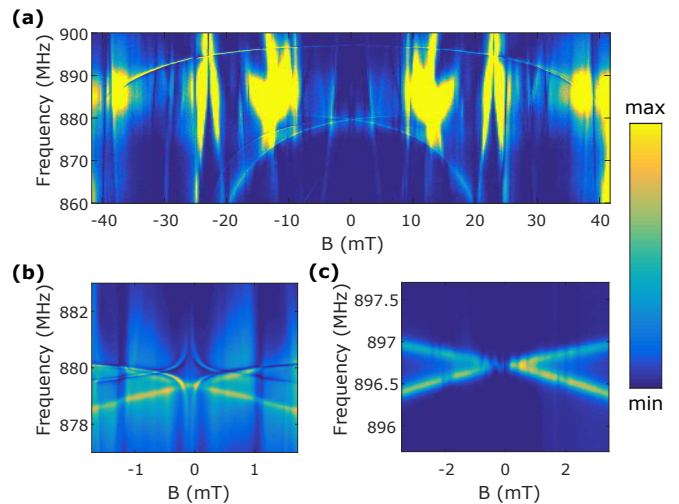


FIG. 2. Raman heterodyne spectra of $^{167}\text{Er}^{3+}:\text{Y}_2\text{SiO}_5$ in an applied magnetic field. Color scales linearly with signal intensity. In (a), the field was applied along the D_1 axis with $\omega_o = 195115.51$ GHz (on average) and the resonator at a temperature (T_{res}) of 4.7 K. In (b) the field was applied along the D_2 axis, with $\omega_o = 195115.67$ GHz and $T_{\text{res}} = 4.8$ K. In (c) the field was applied along the b axis with $\omega_o = 195115.56$ GHz and $T_{\text{res}} = 4.3$ K. Note that the frequency and magnetic field ranges in all three plots are not the same.

the b axis of the crystal.

The resonator is placed inside a homebuilt cryostat (cooling head: Cryomech PT405). A high temperature superconducting vector magnet (HTS-110 Ltd.) provides a magnetic field inside the cryostat.

To perform Raman heterodyne measurements, we use microwaves generated by a network analyzer to drive hyperfine transitions in $^{167}\text{Er}^{3+}:\text{Y}_2\text{SiO}_5$ inside the aforementioned resonator. The resonator is kept at a fixed frequency for these measurements as its linewidth is sufficiently broad such that transitions a few hundred MHz away from the resonant frequency can be detected. The $^4I_{15/2}$ to $^4I_{13/2}$ transition is driven optically with a fiber laser. The Raman heterodyne signal is then detected by a photodiode, and the beat signal is recorded using the same network analyzer. Note that the hyperfine transitions of both the ground and excited state are driven by the resonator, so we are able to measure the hyperfine structure from both electronic states.

An example of the measured Raman heterodyne spectra as a function of magnetic field is shown in Fig. 2, where Fig. 2 (a) shows the spectra for a large range of magnetic field values, and Fig. 2 (b) and (c) show particular transitions of interest for smaller field and frequency ranges. Around 880 MHz [Fig 2 (b)], there are four transitions: a doublet at zero field at 879.4 MHz that appears to be degenerate, and the other two appear over the top, forming a kite-like shape around zero field. The transitions at 879.4 MHz have been reported previously [4],

albeit just as one transition. Figure 2(c) shows the higher frequency transitions, which is another doublet that appears to be degenerate, this time at 896.7 MHz at zero magnetic field.

The aforementioned transitions are not ZEFOZ transitions - close inspection of Fig. 2 (b) and (c) shows that the transitions at 879.4 MHz and 896.7 MHz have some first-order dependence on magnetic field. However, other transitions we found in the 600 to 1200 MHz region that were ZEFOZ transitions had too high curvatures to be suitable for obtaining long coherence times. The transitions at 879.4 MHz and 896.7 MHz had a sufficiently small first-order dependence on magnetic field [see Fig. 2 (a)], so we instead investigated the spin coherence times of these transitions.

To measure the coherence times on these transitions, we use the standard two-pulse spin echo technique [24] as well as a dynamic decoupling pulse sequence [25]. The setup for these pulsed experiments is the same as in Fig. 1, except that instead of the network analyser, a pulsed microwave source is used, and the resulting Raman heterodyne beat signal is analyzed in the time domain by employing a chain of mixers to obtain a 10.7 MHz signal suitable for digitization.

The pulse sequences used are shown in Fig. 3 (a). Initial two-pulse spin echo measurements (RF1) were made on both doublets of selected transitions, with π -pulse lengths of 2 and 6 μ s, and the laser frequencies ω_o of 195115.56 and 195115.67 GHz for the transitions at 879.4 MHz and 896.7 MHz respectively. The frequency of the resonator was tuned to the frequency of the pulses. In order to determine the coherence times, the signal of the echo was analyzed in the Fourier domain. From this, the echo intensities can be determined for different pulse delays τ .

The resulting fitting to the log of the echo intensities can be seen in Fig. 3 (c) and (e). We obtain a value for T_2 by fitting the decay of the echo intensity to $\exp(-4\tau/T_2)$ [26]. Measurements were made at both transition frequencies, and at different temperatures, where the colder measurements yielded longer coherence times - 22 μ s at 4.4 K versus 67 μ s at 3.2 K for $\omega_\mu = 879.4$ MHz, and 80 μ s at 4.6 K versus 300 μ s for $\omega_\mu = 896.7$ MHz.

As can be seen in Fig. 3 (c) and (e), the decay of the two-pulse echoes is not perfectly exponential. This suggests that using a dynamic decoupling pulse sequence (RF2) can extend the coherence time [27]. For these measurements, the same pulse lengths and laser frequencies were used, with $\tau = 17$ and 46 μ s for $\omega_\mu = 879.4$ and 896.7 MHz respectively. Examples of the resulting echoes can be seen in Fig. 3 (b) and (d). The portion of the Raman heterodyne signal that contains the echo is shown in dark blue, with the rest of the signal still visible. There is a clear modulation in the echo envelope that is not present in the two pulse measurements. This is due to the apparent degeneracy of the transitions at

zero field.

Again, the echo signal was analyzed in the Fourier domain, this time determining the echo intensity and thus T_2 for each transition of the doublet separately. An example of the fitting to the echoes is shown in Fig. 3 (c) and (e), where $\tau = 17$ and 46 μ s respectively. These values of τ gave us the longest values T_2 . For $\omega_\mu = 879.4$ MHz, we obtained coherence times of 370 and 380 μ s, and for $\omega_\mu = 896.7$ MHz, 1.45 and 1.37 ms. Although these values for T_2 differ between the members of the same doublet, they are close enough to be the same within experimental error. Comparatively, for the same Er^{3+} concentration, Hashimoto and Shimizu obtained a coherence time of 12 μ s [9].

The main limit to the coherence time in our experiments is the magnetic field fluctuation from Er-Er flip-flops. The large magnetic field and low operating temperature aided in obtaining the long coherence time in [5] by freezing the Er spins. Our results also show this dependence on temperature. Decreasing the concentration of Er^{3+} ions can also reduce the number of Er-Er flip-flops [28]. In the case of the coherent Raman beat analysis on the transitions at 879.4 MHz, decreasing the Er^{3+} ion concentration by a factor of 5 resulted in an increase in sub level coherence by approximately a factor of 4 [9]. In our case, reducing the Er^{3+} ion concentration by a factor of 5 could result in an increase in coherence time by a factor of 25 [29]. In principle, the Er^{3+} ion concentration can be reduced to extend the coherence time until the neighboring yttrium ions become the largest source of dephasing instead.

As the resonator is capable of being tuned over a wide range of frequencies, we measured a plethora of spectra from 600 to 1200 MHz. These spectra can be compared with predictions from recently determined spin Hamiltonian parameters [11] for the hyperfine levels of the $^4I_{15/2}$ state.

One such comparison with our data can be seen in Fig. 4. The doublet at 897.4 MHz is present in the predictions from this spin Hamiltonian, albeit with a shift in the zero field frequency of about 16 MHz. The spin Hamiltonian suggests that there is an avoided crossing between the two transitions, but the size of the avoided crossing is smaller than the linewidths we have observed in our experiments.

Previous hole burning measurements have also identified that the 879.4 MHz transitions are from the ground state [4]. In order to confirm which electronic state the transitions came from, we varied the dark time (τ_d) between turning the laser off and applying the RF pulses. As we increased this delay, the echo from the 896.7 MHz transitions decayed at a rate consistent with the 11 ms excited state lifetime [30], suggesting it comes from the excited state. Comparatively, the echoes from the 879.4 MHz transitions persisted for at least 60 ms, consistent with the previously reported hyperfine lifetime for these

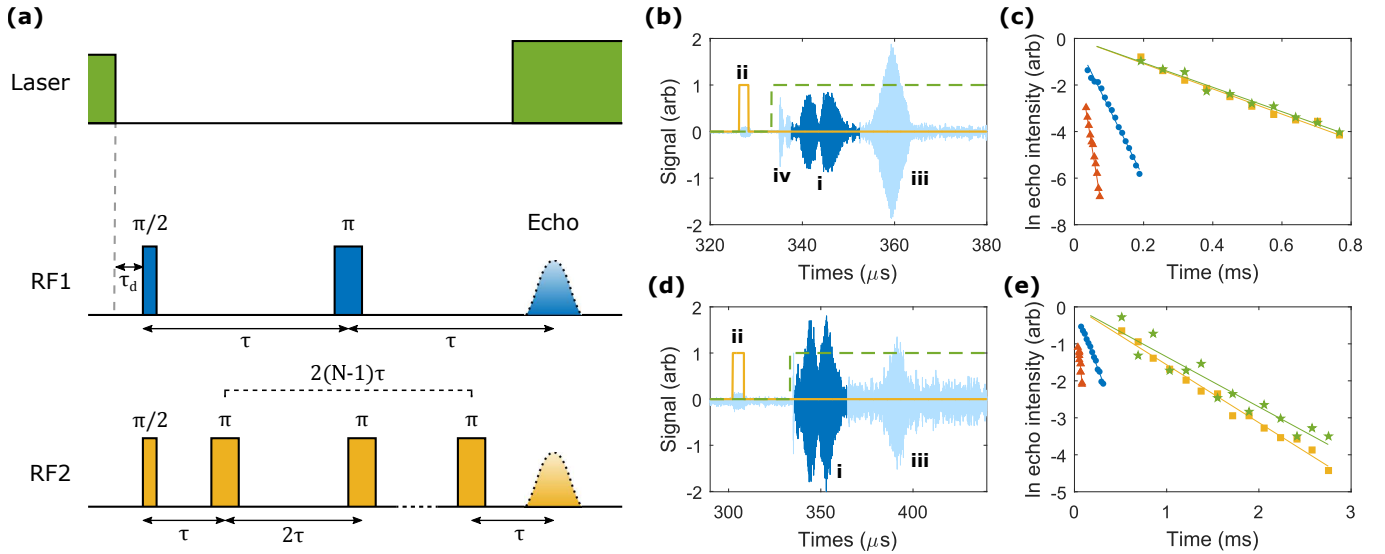


FIG. 3. (a) Pulse sequences used in the echo measurements. For all pulse sequences, the laser is switched off during the RF pulses, and gated on when the echo is expected to appear. RF1 corresponds to the two pulse spin echo sequence, where the delay between pulses τ is varied to obtain the echo height as a function of 2τ . RF2 corresponds to the dynamic decoupling sequence used, where the number of pulses N is increased and the echo height is measured as a function of the total time T since the $\pi/2$ pulse. Examples of echoes from dynamic decoupling (RF2) at (b) 879.4 MHz and (d) 896.7 MHz. The echo (dark blue) indicated by i occurs at a time τ after the final π pulse (ii, yellow). Another echo that comes from the other π pulses is seen at iii in light blue, as well as other noise at iv [(b) only] as a result of the laser (green, dashed line) being turned on. Echo intensities as a function of time since the $\pi/2$ pulse are shown in (c) for 879.4 MHz and (e) for 896.7 MHz. The intensities, and the resulting linear fits come from two pulse echo sequences where $T_{\text{res}} = 4.4, 4.6$ K for (c) and (e) respectively (red, \blacktriangle), $T_{\text{res}} = 3.2$ K for both (c) and (e) (blue, \bullet) and from dynamic decoupling at $T_{\text{res}} = 3.4, 3.3$ K for (c) and (e) respectively (green, \star and yellow, \blacksquare). Relevant pulse durations are given in the main text.

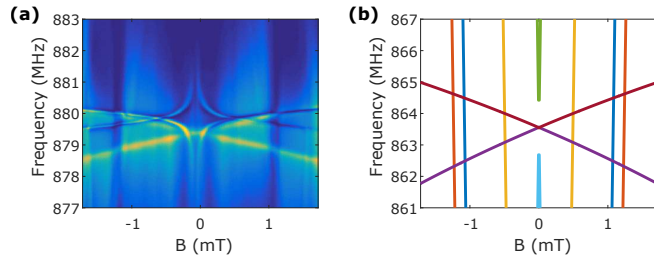


FIG. 4. Comparison between (a) the Raman heterodyne spectra from Fig. 2 (b), and (b) predictions from the spin Hamiltonian from [11] for a magnetic field applied along the D_2 axis. Note that the frequencies along the y axis differ between the two plots, but are on the same scale.

transitions [4]. Note that the 896.7 MHz transitions and the kite-like transitions near 880 MHz are not present in the predictions from the spin Hamiltonian, suggesting they come from the excited state.

We can calculate the strength of the transitions at 879.4 MHz using the spin Hamiltonian [18]. Doing so gives values of 300 and 440 MHz/T for each transition, which is much larger than the nuclear magneton (7.6 MHz/T), i.e., these transitions are stronger than nuclear spin state transitions. The excited state spin Hamiltonian is currently not known, so we cannot calculate the

strengths of the transitions at 896.7 MHz directly. However, we can make an estimate based on the π pulse lengths used in our experiments. This gives a value of about 100 MHz/T.

As we have previously noted [11], additional information at low magnetic fields will significantly improve the predictive power of the ground state spin Hamiltonian parameters. Currently one component of the hyperfine tensor has an uncertainty as large as 45 MHz [11]. Recent EPR measurements taken with a Josephson bifurcation amplifier [31] confirm this. Our data is ideal for resolving these discrepancies as it yields narrow spectral lines and we are able to measure spectra with or without an applied magnetic field.

Using Raman heterodyne, we can determine transition frequencies at a high resolution, where we have typically measured linewidths on the order of 5 MHz and as low as 100 kHz in the case of the transitions at 896.7 MHz. The 100 kHz value is much narrower than the linewidths obtained through conventional EPR, which are on the order of 10s of MHz [10]. This is in line with the observation that ZEFOZ transitions tend to have narrow inhomogeneous linewidths [23, 27]. Presumably the same mechanisms also apply to transitions like those at 879.4 and 896.7 MHz with a small first order Zeeman shift. Standard EPR cannot easily detect these transi-

tions due to the minimal sensitivity of the transitions to changes in magnetic fields.

We have also observed other hyperfine spectra from the excited state besides those shown in Fig. 2. The hyperfine structure of the excited state is largely unknown, so this low field data will be of great benefit to anyone trying to determine the spin Hamiltonian for that state.

To conclude, we have used Raman heterodyne spectroscopy to measure hyperfine spectra from the ground and excited states of $^{167}\text{Er}^{3+}:\text{Y}_2\text{SiO}_5$ as well as to detect spin echoes from both states. Our measurements of the coherence time at zero field are approximately 100 times longer than previous measurements for the same Er^{3+} concentration at zero field [9], and 200 times longer than the coherence time used to demonstrate a microwave memory using the even isotopes of erbium [8]. This demonstrates that $^{167}\text{Er}^{3+}:\text{Y}_2\text{SiO}_5$ is a suitable candidate for a telecom compatible and superconducting qubit compatible microwave quantum memory. The coherence time can still be increased by operating at a lower temperature and lower dopant concentration. With a complete spin Hamiltonian for the ground and excited state, made possible with our spectra obtained through Raman heterodyne, ZEFOZ points can be found to further extend the spin coherence time of $^{167}\text{Er}^{3+}:\text{Y}_2\text{SiO}_5$ with and without an applied magnetic field.

This work was supported by the Marsden Fund of the Royal Society of New Zealand through Contract No. UOO1520.

During the preparation of this manuscript, we became aware of work where Raman heterodyne was used to measure spin echoes on the Kramers' ion $^{171}\text{Yb}^{3+}$ doped in Y_2SiO_5 [32], as well as work where spin echo measurements were made on the excited state of the even Er^{3+} isotopes doped in Y_2SiO_5 [33].

-
- [1] T. Böttger, C. W. Thiel, R. L. Cone, and Y. Sun, *Phys. Rev. B* **79**, 115104 (2009).
- [2] M. Zhong, M. P. Hedges, R. L. Ahlefeldt, J. G. Bartholomew, S. E. Beavan, S. M. Wittig, J. J. Longdell, and M. J. Sellars, *Nature* **517**, 177 (2015).
- [3] E. Fraval, M. J. Sellars, and J. J. Longdell, *Physical Review Letters* **92**, 077601 (2004).
- [4] E. Baldit, K. Bencheikh, P. Monnier, S. Briaudeau, J. A. Levenson, V. Crozatier, I. Lorgeté, F. Bretenaker, J. L. Le Gouët, O. Guillot-Noël, and P. Goldner, *Physical Review B* **81**, 144303 (2010).
- [5] M. Rančić, M. P. Hedges, R. L. Ahlefeldt, and M. J. Sellars, *Nature Physics* **14**, 50 (2018).
- [6] N. Kukharchyk, D. Sholokhov, O. Morozov, S. L. Korableva, A. Kalachev, and P. Bushev, *New Journal of Physics* (2018), 10.1088/1367-2630/aaa7e4.
- [7] D. Bothner, T. Gaber, M. Kemmler, D. Koelle, and R. Kleiner, *Applied Physics Letters* **98**, 102504 (2011).
- [8] S. Probst, H. Rotzinger, A. V. Ustinov, and P. A. Bush, *Phys. Rev. B* **92**, 014421 (2015).
- [9] D. Hashimoto and K. Shimizu, *Journal of Luminescence* **171**, 183 (2016).
- [10] O. Guillot-Noël, P. Goldner, Y. L. Du, E. Baldit, P. Monnier, and K. Bencheikh, *Phys. Rev. B* **74**, 214409 (2006).
- [11] Y.-H. Chen, X. Fernandez-Gonzalvo, S. P. Horvath, J. V. Rakonjac, and J. J. Longdell, *Physical Review B* **97**, 024419 (2018).
- [12] J. Mlynek, N. C. Wong, R. G. DeVoe, E. S. Kintzer, and R. G. Brewer, *Phys. Rev. Lett.* **50**, 993 (1983).
- [13] N. C. Wong, E. S. Kintzer, J. Mlynek, R. G. DeVoe, and R. G. Brewer, *Phys. Rev. B* **28**, 4993 (1983).
- [14] J. J. Longdell, M. J. Sellars, and N. B. Manson, *Physical Review B* **66**, 035101 (2002).
- [15] J. J. Longdell, A. L. Alexander, and M. J. Sellars, *Physical Review B* **74**, 195101 (2006).
- [16] M. Lovrić, P. Glasenapp, D. Suter, B. Tumino, A. Ferrier, P. Goldner, M. Sabooni, L. Rippe, and S. Kröll, *Physical Review B* **84**, 104417 (2011).
- [17] M. Lovrić, P. Glasenapp, and D. Suter, *Physical Review B* **85**, 014429 (2012).
- [18] D. L. McAuslan, J. G. Bartholomew, M. J. Sellars, and J. J. Longdell, *Phys. Rev. A* **85**, 032339 (2012).
- [19] X. Fernandez-Gonzalvo, Y.-H. Chen, C. Yin, S. Rogge, and J. J. Longdell, *Physical Review A* **92**, 062313 (2015).
- [20] R. M. Macfarlane, T. L. Harris, Y. Sun, R. L. Cone, and R. W. Equall, *Optics Letters* **22**, 871 (1997).
- [21] C. Li, C. Wyon, and R. Moncorgé, *IEEE Journal of Quantum Electronics* **28**, 1209 (1992).
- [22] W. N. Hardy and L. A. Whitehead, *Review of Scientific Instruments* **52**, 213 (1981).
- [23] Y.-H. Chen, X. Fernandez-Gonzalvo, and J. J. Longdell, *Phys. Rev. B* **94**, 075117 (2016).
- [24] E. L. Hahn, *Physical Review* **77**, 297 (1950).
- [25] H. Y. Carr and E. M. Purcell, *Physical Review* **94**, 630 (1954).
- [26] P. T. Callaghan, *Principles of Nuclear Magnetic Resonance Microscopy* (Oxford Science Publications, 1991); A. A. Kaplyanskii and R. M. Macfarlane, *Spectroscopy of Solids Containing Rare Earth Ions*, Modern Problems in Condensed Matter Sciences (North-Holland Physics Publishing, 1987).
- [27] E. Fraval, M. J. Sellars, and J. J. Longdell, *Phys. Rev. Lett.* **95**, 030506 (2005).
- [28] T. Böttger, C. W. Thiel, Y. Sun, and R. L. Cone, *Physical Review B* **73**, 075101 (2006).
- [29] J. Rakonjac, *Low-Field ZEFOZ Transitions in Erbium-167-Doped Yttrium Orthosilicate*, Honours Dissertation, University of Otago (2016).
- [30] T. Böttger, Y. Sun, C. W. Thiel, and R. L. Cone, *Physical Review B* **74**, 075107 (2006).
- [31] R. P. Budoyo, K. Kakuyanagi, H. Toida, Y. Matsuzaki, W. J. Munro, H. Yamaguchi, and S. Saito, *Physical Review Materials* **2**, 011403 (2018).
- [32] A. Ortu, A. Tiranov, S. Welinski, F. Fröwis, N. Gisin, A. Ferrier, P. Goldner, and M. Afzelius, arXiv:1712.08615 [cond-mat, physics:physics, physics:quant-ph] (2017).
- [33] S. Welinski, P. J. T. Woodburn, N. Lauk, R. L. Cone, C. Simon, P. Goldner, and C. W. Thiel, arXiv:1802.03354 [quant-ph] (2018).